# A multi-component toxin from *Bacillus cereus* incites inflammation and shapes host outcome via the NLRP3 inflammasome

**Anukriti Mathur**[1], **Shouya Feng**[1], **Jenni A. Hayward**[1], **Chinh Ngo**[1], **Daniel Fox**[1], **Ines I. Atmosukarto**[2], **Jason D. Price**[2], **Kristina Schauer**[3], **Erwin Märtlbauer**[3], **Avril A.B. Robertson**[4], **Gaetan Burgio**[1], **Edward M. Fox**[5], **Stephen H. Leppla**[6], **Nadeem O. Kaakoush**[7], **Si Ming Man**[1,*]

[1]Department of Immunology and Infectious Disease, The John Curtin School of Medical Research, The Australian National University, Canberra, Australia.

[2]Lipotek Pty Ltd. The John Curtin School of Medical Research, The Australian National University, Canberra, Australia.

[3]Department of Veterinary Sciences, Faculty of Veterinary Medicine, Ludwig-Maximilians-Universität München, Oberschleißheim, Germany.

[4]School of Chemistry and Molecular Biosciences, The University of Queensland, Brisbane, Queensland 4072, Australia.

[5]Commonwealth Scientific and Industrial Research Organisation (CSIRO) Agriculture and Food, Private Bag 16, Werribee, Victoria, Australia.

[6]Microbial Pathogenesis Section, Laboratory of Parasitic Diseases, National Institute of Allergy and Infectious Diseases, National Institutes of Health, Bethesda, MD 20892, USA.

[7]School of Medical Sciences, UNSW Sydney, Sydney, NSW, 2052, Australia.

## Abstract

Host recognition of microbial components is essential in mediating an effective immune response. Cytosolic bacteria must secure entry into the host cytoplasm to facilitate replication, and in doing so, liberating microbial ligands which activate cytosolic innate immune sensors and the inflammasome. Here, we identified a multi-component enterotoxin hemolysin BL (HBL) which

*Correspondence: Si Ming Man, *Department of Immunology and Infectious Disease, The John Curtin School of Medical Research, The Australian National University, Canberra, 2601, Australia.* Tel: (61) 2 612 56793, siming.man@anu.edu.au.

AUTHOR CONTRIBUTIONS

A.M. and S.M.M. conceptualized the study; A.M., S.F., J.A.H., C.N., D.F., I.I.A., J.D.P., and N.O.K. performed the experiments; A.M., S.F., J.A.H., C.N., D.F., and N.O.K. conducted the analysis; A.M. and S.M.M. wrote the manuscript. S.M.M. acquired the funding; I.I.A., J.D.P., E.M., A.A.B.R, G.B., E.M.F. and S.H.L. provided resources and intellectual input; S.M.M. provided overall supervision. All authors reviewed the manuscript.

COMPETING INTERESTS

I.I.A. is Director of Lipotek, a niche biotech company with a focus on liposome technology. I.I.A. and J.D.P. are shareholders of Lipotek. A.A.B.R. is inventor on inflammasome inhibitor patents (WO2017140778 and WO2016131098).

Data availability

The data that support the findings of this study are included in this published article along with its Supplementary Information files, and are also available from the corresponding author upon request.

engages activation of the inflammasome. This toxin is highly conserved among the human pathogen *Bacillus cereus*. The three subunits of HBL bind to the cell membrane in a linear order, forming a lytic pore and inducing activation of the NLRP3 inflammasome, secretion of IL-1β and IL-18, and pyroptosis. Mechanistically, the HBL-induced pore results in efflux of potassium and triggers activation of the NLRP3 inflammasome. Further, HBL-producing *B. cereus* induces rapid inflammasome-mediated mortality. Pharmacological inhibition of the NLRP3 inflammasome using MCC950 prevents *B. cereus*-induced lethality. Overall, our results reveal that cytosolic sensing of a toxin is central to the innate immune recognition of infection. Therapeutic modulation of this pathway enhances host protection against deadly bacterial infections.

## INTRODUCTION

Inflammasomes are innate immune signaling complexes capable of responding to a variety of pathogens and danger signals [1,2]. Pathogen-associated molecular patterns (PAMPs) and danger-associated molecular patterns (DAMPs) can be recognized by inflammasome sensors, which on activation recruit the adaptor protein ASC (also known as apoptosis-associated speck-like protein containing a caspase activation and recruitment domain), and the cysteine protease caspase-1 to form a functional inflammasome complex [3,4]. Activation of caspase-1 leads to proteolytic processing and secretion of the pro-inflammatory cytokines Interleukin (IL)-1β and IL-18, and cleavage of the pro-pyroptotic executioner gasdermin D leading to the induction of an inflammatory form of cell death known as pyroptosis [5]. These cellular processes regulate host defense against pathogens.

Recognition of PAMPs and DAMPs by inflammasome sensors requires cytosolic exposure of microbial or danger signals. Cytosolic bacterial invasion is central to drive activation of the DNA-sensing AIM2 inflammasome and the LPS-sensing non-canonical inflammasome. This process is initiated by host defense proteins, guanylate-binding proteins and Immunity-related GTPases, mediating a rupture of the pathogen-containing vacuole and liberating bacterial ligands in the cytoplasm [6–9]. Certain pathogens inject virulence factors into the cytoplasm, such as flagellin delivered by the type III secretion system of *Salmonella enterica* serovar Typhimurium (*S.* Typhimurium), which induces activation of the NAIP-NLRC4 inflammasome [10–15]. However, the mechanisms underpinning how microbial ligands from extracellular bacteria are detected by cytosolic innate immune sensors have remained unclear.

Toxins are critical tools in the arsenal of bacterial virulence factors which can modify the function, metabolism and physiology of the host cell to favor bacterial replication and transmission [16,17]. Previous studies have shown that hemolysins and β-barrel pore-forming toxins secreted by *Staphylococcus aureus* induce activation of the NLRP3 inflammasome in monocytes and macrophages [18–21]. Similarly, hemolysins secreted by *Escherichia coli* [22,23], *Streptococcus pneumoniae* [24–28], *Listeria monocytogenes* [18,29,30] and certain *Vibrio* species [31–33] can activate the NLRP3 inflammasome. The mechanisms governing how inflammasome sensors recognize such a structurally and mechanistically diverse family of virulence factors are unclear.

Here, we analyzed a panel of extracellular and cytosolic bacterial pathogens and identified an activator of the inflammasome secreted by the foodborne pathogen *Bacillus cereus*. We showed that the secreted factor is a tripartite toxin called hemolysin BL (HBL). HBL assembled in a highly sequential manner to drive activation of the NLRP3 inflammasome. We also demonstrated that the HBL toxin is inserted into the mammalian cell membrane to form a pore, mediating cellular leakage and lysis. Overt activation of the HBL-responsive NLRP3 inflammasome drives rapid death of the host, which can be prevented by pharmacological inhibition of NLRP3. Our results revealed that cytosolic sensing of an inflammasome-activating toxin is central to the immune recognition of *B. cereus* infection.

## RESULTS

### A secreted bacterial factor induces activation of the inflammasome

We and others have previously demonstrated that certain intracellular bacteria must secure entry into the host cytoplasm such that bacterial ligands are liberated via a host-mediated process for innate immune recognition by inflammasome sensors [6–9]. Indeed, wild-type (WT) bone-marrow-derived macrophages (BMDMs) infected with a range of clinically important bacterial pathogens undergo activation of caspase-1, secretion of IL-1β and IL-18, and induction of pyroptosis (Fig. 1a,b). The cell-free supernatant from most bacteria was unable to induce activation the inflammasome (Fig. 1a,b). The cell-free supernatant derived from *B. cereus* induced robust activation of caspase-1, secretion of IL-1β and IL-18, and pyroptosis (Fig. 1a,b).

To identify the inflammasome sensor required to activate the inflammasome in response to the secreted factor of *B. cereus*, we stimulated LPS-primed BMDMs with the supernatant of *B. cereus*. Activation of caspase-1, the release of IL-1β and IL-18, and induction of cell death were impaired in *Nlrp3*$^{-/-}$ and *Asc*$^{-/-}$ BMDMs stimulated with the supernatant of *B. cereus* compared with WT, *Nlrc4*$^{-/-}$, *Aim2*$^{-/-}$, and *Casp11*$^{-/-}$ BMDMs (Fig. 1c–e and Supplementary Fig. 1a). The supernatant of *B. cereus* similarly induced activation of the NLRP3 inflammasome in unprimed BMDMs (Supplementary Fig. 1b), suggesting that Signal 1 (priming) and Signal 2 (activation) were both provided by the supernatant of *B. cereus*.

We further found that *B. cereus* infection activated the inflammasome in a manner dependent on NLRP3 (Figs. 1c–e). The secreted levels and gene expression of the pro-inflammatory cytokines tumor-necrosis factor (TNF) and Keratinocyte chemoattractant (KC, also known as CXCL1) and the phosphorylation status of IκB and ERK between WT and *Nlrp3*$^{-/-}$ BMDMs infected with *B. cereus* were similar (Supplementary Fig. 1c–e). These data confirmed that the production of inflammasome-independent cytokines was not affected by the absence of NLRP3. Further, pharmacological blockade of NLRP3 using the small molecule inhibitor MCC950 [34], impaired activation of the inflammasome in BMDMs infected with *B. cereus* or stimulated with LPS+ATP (Supplementary Fig. 1f).

Formation of the ASC speck is a hallmark of inflammasome activation [35]. Indeed, we found that *Nlrp3*$^{-/-}$ BMDMs had an impaired ability to generate ASC specks in response to stimulation with the supernatant of *B. cereus* or infection with *B. cereus*, but not in response

to transfected dsDNA poly(dA:dT) (Fig. 1f). These results collectively suggested that a secreted factor produced by *B. cereus* induces activation of the NLRP3 inflammasome.

## The secreted factor is a heat-sensitive protein of 30–50 kDa in size

To investigate the biological nature of the unknown inflammasome-activating factor, we stimulated BMDMs with the supernatant of *B. cereus* treated with 100 °C heat, proteinase K, DNase, or RNase. Treatment with heat or proteinase K, but not with DNase or RNase, abolished the ability of the supernatant of *B. cereus* to engage activation of the inflammasome (Supplementary Fig. 2a). Further, the supernatant heated to 50 °C, but not 75 °C, retained its ability to activate inflammasome responses (Supplementary Fig. 3a,b). Consistent with this finding, heat-killed or paraformaldehyde-fixed *B. cereus* bacteria were unable to induce activation of the inflammasome (Supplementary Fig. 2b), suggesting that the bacteria must be viable, secreting a heat-sensitive proteinaceous factor that engages activation of the NLRP3 inflammasome. Size-fractionation of the supernatant revealed that the fractions of >9, >30 and <50 kDa, induced activation of the inflammasome (Supplementary Fig. 2c–e). Collectively, these findings suggested that a heat-sensitive proteinaceous factor of 30–50 kDa secreted by *B. cereus* is an activator of the NLRP3 inflammasome.

## The secreted factor is highly prevalent in *B. cereus* strains

To unravel the identity of the secreted factor, we comprehensively profiled a collection of 46 strains of *B. cereus*, for their ability to activate the inflammasome (Supplementary Table 1). The supernatant and bacteria from 91% (42/46) of the strains triggered activation of caspase-1 and secretion of IL-1β and IL-18 in WT BMDMs (Fig. 2a,b and Supplementary Fig. 4a,b), suggesting that the secreted factor is highly prevalent amongst *B. cereus* isolates. Notably, *Nlrp3*$^{-/-}$ BMDMs did not undergo activation of caspase-1 or release of IL-1β and IL-18 in response to any of the supernatant or bacteria (Figs. 2a,b and Supplementary Fig. 4a,b), suggesting that NLRP3 is the cytosolic sensor driving inflammasome-mediated immune detection of this bacterial species. The 4 non-activating strains and their supernatant did not induce pyroptosis, but induced the secretion of TNF (Fig. 2c and Supplementary Fig. 4c). These results suggested that the non-activating strains are not globally defective in eliciting an inflammatory response. In addition, the distinction between an “inflammasome-activating” and “non-activating” group of *B. cereus* allows us to elucidate key genetic and proteomic differences to facilitate identification of this inflammasome-activating secreted factor.

## Identification of the inflammasome-activating factor

*B. cereus*, secretes multiple toxins, including the toxins non-hemolytic enterotoxin (NHE), hemolysin BL (HBL), and Cytotoxin K [36]. Individual components of the two tripartite toxins NHE (composed of A, B and C) and HBL (composed of B, $L_1$ and $L_2$), and the single-component toxin, Cytotoxin K, are all of 30–50 kDa in size [37–41]. Real-time qPCR analysis revealed that the genes *hblA*, *hblC* and *hblD*, encoding B, $L_2$ and $L_1$ respectively, were expressed in inflammasome-activating strains, but not in non-activating strains (Fig. 2d). In addition, we did not observe any association between the expression levels of genes

encoding NheB and Cytotoxin K and the ability of the strains to activate the inflammasome (Supplementary Fig. 4d).

Duopath analyses revealed that the supernatant of 42 inflammasome-activating strains, but not the 4 non-activating strains, were positive for HBL (Fig. 2e and Supplementary Fig. 4e), whereas NHE was present in the supernatant of all 46 strains (Fig. 2e and Supplementary Fig. 4e). Furthermore, the supernatant of inflammasome-activating strains were positive for the HBL components, whereas the non-activating strains lacked HBL components (Fig. 2f). These data collectively highlighted that the secretion of the enterotoxin HBL is a feature of inflammasome-activating strains of *B. cereus*.

## HBL activates the NLRP3 inflammasome

The presence of HBL exclusively in inflammasome-activating strains suggested that this enterotoxin might activate the NLRP3 inflammasome. To investigate this possibility, we infected BMDMs with *B. cereus* and its isogenic mutant lacking HBL (Δ*Hbl B. cereus*). We observed that the parental strain and its supernatant induced activation of the inflammasome in WT BMDMs, but not in *Nlrp3*$^{-/-}$ BMDMs, whereas the Δ*Hbl B. cereus* and its supernatant failed to induce these responses (Fig. 3a,b). Indeed, we confirmed that the Δ*Hbl B. cereus* lacked the expression of HBL, but retained the expression of NHE and Cytotoxin K (Fig. 2c–e, Fig. 3c and Supplementary Fig. 5a). Both the parental and Δ*Hbl* strains of *B. cereus* induced similar levels of TNF (Fig. 3b). In addition, we found that the supernatant neutralized with anti-HBL antibodies did not induce activation of the inflammasome, but retained the ability to induce TNF production (Fig. 3f).

## Deficiency of NHE or Cytotoxin K does not impair activation of the NLRP3 inflammasome

To investigate potential contributions from NHE in the activation of the inflammasome, we infected BMDMs with *B. cereus* and its isogenic mutant lacking NHE (Δ*Nhe B. cereus*). We found that Δ*Nhe B. cereus* or its supernatant retained the ability to engage activation of the NLRP3 inflammasome (Fig. 3g–k). Indeed, Δ*Nhe B. cereus* expressed HBL and Cytotoxin K (Supplementary Fig. 5b). Further, treatment of the supernatant with anti-NHE neutralizing antibody did not impair activation of the inflammasome (Fig. 3l). However, addition of neutralizing antibodies against HBL abolished the ability of the supernatant from Δ*Nhe B. cereus* to elicit inflammasome responses (Supplementary Fig. 5c).

We also quantified the mRNA levels of Cytotoxin K in eight *B. cereus* strains. Two of these strains, strains #34 and #44, had impaired expression of Cytotoxin K (Supplementary Fig. 4d). These two strains retained the ability to induce activation of the inflammasome (Fig. 2a,b and Supplementary Fig. 4a,b). Further, we identified a Cytotoxin K-expressing strain, strain #43 (Supplementary Fig. 4d) which was unable to induce activation of the NLRP3 inflammasome, presumably owing to a lack of expression of HBL (Fig. 2a,b,d and Supplementary Fig. 4a,b). These studies collectively suggested that HBL, but not NHE or Cytotoxin K, is the secreted factor of *B. cereus* activating the NLRP3 inflammasome.

## Sequential assembly of HBL components is required to activate the inflammasome

The tripartite enterotoxin HBL is composed of a 37–41 kDa component B, a 38–42 kDa component $L_1$, and a 43–47 kDa component $L_2$ [37–40]. We found that recombinant HBL induced robust activation of the inflammasome in WT BMDMs, but not in *Nlrp3*$^{-/-}$ BMDMs (Fig. 4a). The inflammasome activating ability of HBL was abolished by treating with heat or proteinase K (Supplementary Fig. 6a). Importantly, either individual or combination of two of the three components of HBL were unable to engage activation of the inflammasome (Fig. 4a,b). Further, neutralization of a single component, using antibodies impaired inflammasome activation induced by *B. cereus* supernatant (Fig. 4c). These results suggested that all three components of HBL were necessary to drive activation of the NLRP3 inflammasome.

A previous study has shown that B, $L_1$ and $L_2$ can bind sheep red blood cells independently of one another [42], whereas another study has found that B, $L_1$ and $L_2$ assemble on Chinese Hamster Ovary cells in a sequential manner [40]. Investigation of a specific order of toxin assembly demonstrated that addition of B, followed by $L_1$+$L_2$ induced robust inflammasome activation (Fig. 4d). These findings indicated that component B is the apical component initiating HBL assembly and activation of the NLRP3 inflammasome. To identify the precise order of toxin assembly, we added to BMDMs each component in the order of B→$L_1$→$L_2$ or B→$L_2$→$L_1$. Of the two orders, only B→$L_1$→$L_2$ triggered inflammasome activation (Fig. 4e). Therefore, a highly specific and linear order of HBL assembly is required to activate the NLRP3 inflammasome.

## Cytosolic access of HBL components is not required to engage activation of the inflammasome

Previous studies demonstrated that the anthrax lethal toxin of *Bacillus anthracis,* a phylogenetic neighbor of *B. cereus,* requires cytosolic access to activate the NLRP1 inflammasome [43–45]. To investigate whether activation of the NLRP3 inflammasome is mechanistically dependent on cytosolic access of HBL components, we inhibited phagocytosis of macrophages. Treatment of BMDMs with cytochalasin B or cytochalasin D did not impair the ability of HBL, the supernatant of *B. cereus*, or live *B. cereus* to induce activation of the inflammasome (Supplementary Fig. 6b,c). In contrast, treatment of BMDMs with cytochalasin B or cytochalasin D impaired activation of the inflammasome by *S.* Typhimurium (Supplementary Fig. 6c), consistent with our previous findings [46]. Further, transfection of HBL components into BMDMs was unable to induce inflammasome activation, whereas transfection of flagellin activated inflammasome responses (Fig. 4f). These findings suggested that, unlike anthrax lethal toxin, cytosolic entry of HBL components is not necessary to engage activation of the NLRP3 inflammasome. Furthermore, we found that both WT and *Casp11*$^{-/-}$ BMDMs underwent similar levels of inflammasome activation (Supplementary Fig. 6d), confirming that activation of the NLRP3 inflammasome is not owing to HBL-mediated transportation of LPS to activate the caspase-11 non-canonical inflammasome.

### HBL components assemble on the cell membrane to induce pores and cell lysis

The important observation that only the 30–50 kDa supernatant fraction activated the inflammasome excluded the possibility that HBL forms a bipartite or tripartite toxin complex in solution (Supplementary Fig. 2c–e). Our binding studies further supported the idea that an apical component must bind to the plasma membrane prior to the next component being recruited (Fig. 4d,e). Indeed, we separated the cell-membrane and cytosolic fractions of BMDMs stimulated with HBL or the supernatant of *B. cereus* and found that HBL components remained in the cell-membrane fraction (Fig. 4g). Further, immunofluorescence staining revealed that the B component of HBL and the cell surface marker CD11b co-localized on the membrane of BMDMs (Fig. 4h).

To identify the mechanisms of action for HBL on the cell membrane, liposomes mimicking the mammalian cell membrane were treated with HBL. Indeed, addition of HBL, but not heat-inactivated or individual components of HBL, induced robust leakage of the liposome-encapsulated dye (Fig. 5a). Further, addition of liposomes sequestered the toxin and completely abolished the ability of HBL to induce activation of the inflammasome (Fig. 5b).

The observations that HBL has the capacity to insert into liposomal membranes led us to use bioinformatic tools to search for transmembrane regions in HBL components. We found a putative transmembrane region corresponding to residues 232 to 250 in the protein sequence of component B (Supplementary Fig. 7a,b). This analysis is consistent with a previous study reporting the presence of a transmembrane region in component B [47]. We further identified two putative transmembrane regions in component $L_1$, corresponding to residues 243 to 261, and residues 329 to 347 (Supplementary Fig. 7a,c). Indeed, the transmembrane amphipathic helix of B contains a highly conserved proline residue, which is present in transmembrane α-helices and essential for inducing hinge or distortion in the membrane helix for normal functioning of certain transmembrane channels [48–51](Supplementary Fig. 7b). We also identified a signal peptide in the N-terminus of B, $L_1$ and $L_2$ (Supplementary Fig. 7a), confirming the secretory nature of HBL.

No studies have reported visualization of a toxin pore induced by HBL. Cryo-electron microscopy analysis (Cryo-EM) revealed distinct membrane pores in the membrane of liposomes treated with HBL (Fig. 5c). Further, Scanning Electron Microscopy showed that BMDMs treated with *B. cereus* or HBL or the supernatant showcased features of a pyroptotic cell including loss of membrane integrity, cytoplasm rounding, a centralized nucleus in a deflated cell body (Fig. 5d and Supplementary Fig. 8). Untreated BMDMs exhibited a prominent cell body composed of membrane ruffles and projections (Fig. 5d and Supplementary Fig. 8). We also observed phagocytosed bacteria being expelled following membrane rupture (Fig. 5d), consistent with previous findings [52,53]. Transmission Electron Microscopy further revealed a loss of cytoplasmic content and nuclear condensation in BMDMs stimulated either with HBL or the supernatant of *B. cereus* (Fig. 5e).

To investigate whether the toxin can directly induce a rupture of the cell membrane, we monitored, using IncuCyte, dynamics of the viability of WT and *Nlrp3*$^{-/-}$ BMDMs exposed to HBL. A low concentration of 5 nM HBL triggered activation of caspase-1, cleavage of gasdermin D and IL-1β, secretion of IL-1β and IL-18, and cell death in WT BMDMs, but

not in *Nlrp3*$^{-/-}$ BMDMs (Supplementary Fig. 9a-c). In contrast, a high concentration of 0.5 μM HBL induced very rapid cell death in both WT and *Nlrp3*$^{-/-}$ BMDMs within 20 min but failed to trigger activation of the inflammasome (Supplementary Fig. 9a-c). Collectively, these findings indicated that HBL binds and orchestrates disruption of the cell membrane, leading to rapid cell lysis or activation of the NLRP3 inflammasome in a manner dictated by the bioavailability and concentration of HBL.

## HBL-induced activation of the inflammasome requires $K^+$ efflux

Pore-forming toxins have the capacity to alter intracellular homeostasis. Indeed, efflux of $K^+$ has been proposed to be a central mechanism by which the NLRP3 inflammasome can be activated [54]. We observed that addition of extracellular $K^+$ inhibited activation of the inflammasome in a dose-dependent manner in response to recombinant HBL, the supernatant of *B. cereus* or *B. cereus* (Supplementary Fig. 10a,b). Addition of extracellular $K^+$ also inhibited activation of the inflammasome by LPS+ATP (Supplementary Fig. 10a,b), consistent with previous studies [55–57].

## Pharmacological inhibition of NLRP3 prevents *B. cereus*-induced lethality

We further investigated the role of the NLRP3 inflammasome in host defense against *B. cereus* infection *in vivo.* We observed that only 40% (10/25) of the WT mice survived the infection, whereas 92% (12/13) of the *Nlrp3*$^{-/-}$ mice and 81% (13/16) of the *Casp1/11*$^{-/-}$ mice survived (Fig. 6a). Analysis of the serum showed that *Nlrp3*$^{-/-}$ and *Casp1/11*$^{-/-}$ infected mice had a reduced level of IL-18 compared to infected WT mice (Fig. 6b). Similarly, administration of the supernatant of *B. cereus* induced IL-18 in the serum of WT mice; levels of IL-18 in *Nlrp3*$^{-/-}$ and *Casp1/11*$^{-/-}$ mice were significantly reduced (Fig. 6c). We speculate that the residual levels of IL-18 observed in mice lacking NLRP3 might be due to contributions from another inflammasome sensor.

To confirm a role for HBL in the pathogenesis of *B. cereus* infection *in vivo*, we infected WT mice either with WT or Δ*Hbl B. cereus*. A higher percentage of WT mice survived when infected with Δ*Hbl B. cereus* (87%, 13/15) compared to mice infected with WT *B. cereus* (25%, 4/16) (Fig. 6d). Further, WT mice infected with Δ*Hbl* produced substantially less IL-18 in the peritoneal fluid and serum compared with WT mice infected with WT *B. cereus* (Fig. 6e,f).

Given that activation of the NLRP3 inflammasome in response to *B. cereus* infection resulted in rapid lethality in mice (Fig. 6a), we hypothesized that pharmacological blockade of the NLRP3 inflammasome would yield a beneficial outcome in the host. Indeed, all (14/14) of the MCC950-treated mice survived the infection, whereas only 23% (3/13) of the PBS-treated mice survived (Fig. 6g), suggesting that MCC950-mediated inhibition of the NLRP3 inflammasome completely protected WT mice from *B. cereus*-induced lethality. Further, administration of MCC950 to WT mice infected with *B. cereus* attenuated secretion of IL-18 in the peritoneal cavity and circulation, whereas administration of PBS did not (Fig. 6h,i). Together, these results highlighted that *B. cereus* infection induces activation of the NLRP3 inflammasome *in vivo* and that therapeutic blockade of the NLRP3 inflammasome efficiently rescued mice from *B. cereus*-induced mortality.

## DISCUSSION

Activation of the inflammasome is one of the hallmarks of innate immune recognition of pathogens and danger signals. We and others have shown that cytosolic bacteria, such as *F. novicida* and *L. monocytogenes*, must escape the pathogen-containing vacuole to the cytoplasm of the host cell in order to induce activation of cytosolic inflammasome sensors [6,7,58,59]. However, the mechanisms governing how secreted bacterial factors are detected by innate immune sensors in the cytosol in the absence of bacterial invasion have remained largely unknown.

Our studies revealed that the multi-component toxin HBL produced by the foodborne pathogen *B. cereus* is recognized by the cytosolic sensor NLRP3 (Supplementary Fig. 11). Identification of a role for the inflammasome in *B. cereus* infection and the specific microbial activator triggering inflammasome responses have several important implications. *B. cereus* is a ubiquitous spore-forming foodborne pathogen of humans. Ingestion of toxins secreted by *B. cereus* is sufficient to result in vomiting and/or diarrhoea [60], suggesting that toxins of *B. cereus* are strong inducers of gastrointestinal inflammation. In addition, *B. cereus* can cause a range of often-lethal extra-gastrointestinal infections, including sepsis, pneumonia, and meningitis [36]. Despite the clinical importance of *B. cereus* in humans, little is known about the role of the immune system in host defense against this pathogen.

Our studies revealed a physiological relevance of the inflammasome pathway in the pathogenesis of *B. cereus* infection. Activation of the NLRP3 inflammasome leads to overt inflammation that may drive immunopathology and septic shock in *B. cereus*-infected mice, resulting in rapid lethality reminiscent of LPS-induced endotoxemia [61]. Of clinical importance is the therapeutic benefit of inhibiting the NLRP3 inflammasome using the inhibitor MCC950 [34]. Administration of MCC950 completely prevented lethality induced by *B. cereus* infection in mice, highlighting its ability to dampen detrimental inflammasome activity triggered by fulminant bacterial infections. A therapeutic application for MCC950 has been demonstrated in mouse models of cryopyrin-associated periodic syndromes, skin inflammation, multiple sclerosis, non-alcoholic fatty liver disease, and certain viral infections [34,62–65].

In addition to inflammasome inhibition, administration of small-molecule inhibitors or antibody-mediated neutralization against HBL of *B. cereus* might prevent lethality. Indeed, previous studies have shown that pharmacological inhibition or antibody-mediated neutralization against the anthrax toxin can prevent lethal infection by *B. anthracis* [66,67]. These studies would suggest that targeting bacterial toxins could be a highly effective and universal strategy in the prevention and treatment of infection by toxin-producing bacteria.

Our studies revealed that component B of HBL is the apical subunit initiating assembly of the HBL pore on cell membrane, followed by recruitment of $L_1$ and $L_2$. We hypothesize that attachment of B on the macrophage cell membrane induces a conformation change that enables recruitment of $L_1$. Indeed, a previous study have suggested that B can oligomerize on the cell membrane [47]. $L_1$ might also anchor to the cell membrane owing to its two

putative transmembrane helices, forming a stable B-$L_1$ platform mediating the recruitment of the final component, $L_2$.

Previous studies have shown that both HBL and NHE are tripartite pore-forming toxins [42,68]. The structure of HBL-B [47] and NHE-A [69] have been elucidated, showing that both are α-pore-forming toxins. Our data revealed that HBL-induced activation of the NLRP3 inflammasome requires $K^+$ efflux. A previous study has shown that the NHE pore is also permeable to $K^+$ [70]. The NHE pore has a predicted diameter of 5 nm [70] whereas the HBL pore has a diameter of 1.2 nm [42]. The different diameters of the pores between HBL and NHE might affect their overall ion selectivity, and therefore, their ability to induce activation of the inflammasome.

In conclusion, we identified NLRP3 as the cytosolic innate immune sensor of the human foodborne pathogen *B. cereus*. We also identified the multi-component toxin HBL as an activator of the inflammasome and a virulence factor which drives inflammasome-mediated lethality *in vivo*. Our results further highlight that pharmacological inhibition of inflammasomes is a highly effective therapeutic option in potentially lethal bacterial infections.

## METHODS

### Mice

*Aim2*$^{-/-}$ [71], *Asc*$^{-/-}$ [10], *Casp1/11*$^{-/-}$ [72], *Casp11*$^{-/-}$ [73], *Nlrp3*$^{-/-}$ [74], and *Nlrc4*$^{-/-}$ [10] mice have been described previously. All mice are on the C57BL/6 background. Male and female mice of 6–8 weeks old were used. Mice were bred and maintained at The Australian National University and experiments were conducted under the oversight of The Australian National University Animal Experimentation Ethics Committee, according to the Protocol Number A2017/05.

### Bone Marrow-Derived Macrophages

Primary bone marrow-derived macrophages (BMDMs) were cultured for 5–6 days in DMEM (11995073, ThermoFisher Scientific) supplemented with 10% FBS (F8192, Sigma), 30% L929 conditioned media and 1% penicillin and streptomycin (10378016, Gibco ThermoFisher) as described previously [6]. BMDMs were seeded in antibiotic-free media at a concentration of $1 \times 10^6$ cells per well in 12-well plates.

### Bacterial Culture

*B. cereus* were grown in Luria-Bertani (LB) media (244620, BD) overnight under aerobic conditions at 30 °C. The list of *Bacillus* strains used are mentioned in Supplementary Table 1. *Citrobacter rodentium*, *Escherichia coli, Pseudomonas aeruginosa*, *Salmonella enterica serovar* Typhimurium, *Shigella flexneri*, *Staphylococcus epidermidis*, *Streptococcus pneumoniae*, and *Streptococcus pyogenes* were grown in LB media overnight under aerobic conditions at 37 °C. *Francisella novicida* were cultured in BBL Trypticase Soy Broth (TSB) (211768, BD) supplemented with 0.2% L-cysteine (BP376–100, ThermoFisher Scientific) overnight under aerobic conditions at 37 °C. *Listeria monocytogenes* were grown in Brain

heart infusion (BHI) media (211059, BD) overnight under aerobic conditions at 37 °C. All bacteria were subcultured (1:10) in fresh media the next day for 3–4 hr under their respective conditions.

### Stimulation of BMDMs with Bacteria and Classical Inflammasome Activators

The following conditions were used to stimulate BMDMs: *B. cereus* (MOI 5–10 and 3–6 hr for caspase-1 activation; MOI 2 and 5–60 min for pIkB, IkB, pERK, ERK, NLRP3 and GAPDH expression), *C. rodentium* (MOI 20 for 20 hr), *E. coli* (MOI 20 for 20 hr), *F. novicida* (MOI 100 for 20 hr), *P. aeruginosa* (MOI 2 for 4 hr), *S.* Typhimurium (MOI 2 for 4 hr), *S. flexneri* (MOI 50 for 20 hr), *L. monocytogenes* (MOI 20 for 20 hr), *S. epidermidis* (MOI 50 for 20 hr), *S. pneumoniae* (MOI 50 for 20 hr), and *S. pyogenes* (MOI 50 for 20 hr). 50 μg/ml gentamicin (15750–060, ThermoFisher Scientific) were added after 4 hr (*C. rodentium*, *E. coli*, *S. flexneri*, *L. monocytogenes*, *S. epidermidis*, *S. pneumoniae* and *S. pyogenes*), or 8 hr (*F. novicida*) after the infection to kill extracellular bacteria. Heat-killed *B. cereus* were prepared by heating *B. cereus* to 100 °C for 1 hr. Paraformaldehyde-fixed *B. cereus* were prepared by fixing bacteria in 4% paraformaldehyde for 1 hr.

To activate the canonical NLRP3 inflammasome as controls, BMDMs were primed using 500 ng/ml ultrapure LPS from *E. coli* (ALX-581–014-L002, Enzo Life Sciences) for 4 hr and stimulated with 5 mM ATP (10127531001, Roche) for 45 min. To activate the AIM2 inflammasome, 2.5 μg of poly(dA:dT) (tlrl-patn, InvivoGen) were resuspended in PBS and mixed with 0.3 μl of Xfect polymer in Xfect reaction buffer (631318, Clontech Laboratories, Inc.). After 10 min, DNA complexes were added to BMDMs in Opti-MEM (31985–070, ThermoFisher Scientific) and left stimulated for 5 hr. To activate the NLRC4 inflammasome, *S.* Typhimurium (MOI 2 for 4 hr) or ultrapure flagellin from *S.* Typhimurium (2 μg, tlrl-epstfla-5, InvivoGen) was used. Ultrapure flagellin was mixed with 20 μl of the liposomal transfection reagent DOTAP (11202375001, Sigma) in PBS. After 30 min, the complexes were added to LPS-primed BMDMs in Hank's Balanced Salt Solution (H9394, Sigma) and incubated for 3–5 hr. Cell culture supernatants were collected for ELISA and LDH assays. For inhibition studies, 50 μM of cytochalsin B (C6762, Sigma), 50 μM of cytochalsin D (C8273, Sigma), or 20 μM of the selective and potent inhibitor MCC950 [34] or increasing concentration of potassium chloride (KCl) at 5 mM, 25 mM, 50 mM and 75 mM (P9541, Sigma) were added to BMDMs 30 min prior to stimulation.

### Stimulation of BMDMs with Bacterial Supernatant

To prepare the bacterial supernatant, bacteria were grown in media under their respective conditions as described above. The overnight bacterial culture was centrifuged at 4,500 rpm for 10 min. The supernatant was filter-sterilized using low-protein-binding 0.45 μm filters (SLHV033RS, Merck). For size-fractionation, the supernatant of *B. cereus* was fractionated using spin-filter columns of the 9 kDa (89884A, ThermoFisher Scientific), 30 kDa (UFC803096, Millipore), or 50 kDa range (UFC905096, Millipore). For heat inactivation, the supernatant of *B. cereus* was heated to 50 °C, 75 °C or 100 °C for 10 min. To remove proteins, DNA or RNA, the supernatant of *B. cereus* was treated with Proteinase K (1 mg/ml, 19133, Qiagen), DNase1 (1 mg/ml, Roche), or RNase A (1 mg/ml, Qiagen) for 1 hr. 50–150 μl of bacterial supernatant were added to BMDMs for 3–4 hr.

For neutralization studies, the supernatant of *B. cereus* was treated with antibodies against HBL (3 μl), individual components of HBL (1 μl), or NHE-B (3 μl) for 1 hr before addition to LPS-primed BMDMs. Antibodies against HBL and NHE were generated as described previously [40,75]. For controls, mouse serum and isotype IgG1 were used.

## Stimulation of BMDMs with Recombinant HBL

Purified recombinant HBL components B, $L_1$ and $L_2$ were generated as described previously[40]. LPS-primed BMDMs were stimulated with all three components or with B, $L_1$ or $L_2$ individually or in various combinations (5 nM and 3 hr for caspase-1 activation). HBL components were also pre-incubated with either Proteinase K (1 mg/ml, 19133, Qiagen), DNase1 (1 mg/ml, Roche), or RNase A (1 mg/ml, Qiagen) for 1 hr, or heated to 100 °C for 10 min. For binding order studies, LPS-primed BMDMs were stimulated with a single HBL component (either B, or $L_1$, or $L_2$) for 30 min. This step is followed by extensive washing with PBS three times to remove unbound toxin. The two remaining components were added in concert, or the second individual component was added for 30 min followed by the third individual component, with washing steps in between. The plus symbol indicates ‘added in concert’. The arrow symbol indicates ‘extensive washing’. For transfection of HBL, each reaction consisted of individual HBL components (1.5 μM each) or combination of two components (0.75 μM each) mixed with 10 μl of the liposomal transfection reagent DOTAP (11202375001, Sigma). After 30 min, the complexes were added to LPS-primed BMDMs in Hank’s Balanced Salt Solution (H9394, Sigma) and left stimulated for 3–5 hr.

## Liposome Studies

Liposomes were synthesized using cholesterol (23%) and synthetic lipid derivatives DPPC (33%), DOPC (32%) and DSPC (12%), mimicking the mammalian cell membrane [76]. The concentration of liposomes was 7 mM, loaded either with methylene blue dye (75 μg/ml) or saline. Encapsulation of methylene blue dye into the lumen of liposomes allowed us to investigate the ability of HBL to induce pores in the liposomal membrane that would result in leakage of the dye. Liposomes were treated with HBL (0.5 μM), individual HBL components (0.5 μM), heat-inactivated HBL, a protein buffer used to carry HBL [10 mM Tris HCl, 0.5 mM EDTA (pH 8.0)], or BSA (1 μg/ml; 001000173, Jackson ImmunoResearch). The liposomes were sonicated at 100 amplitude for 5 mins as control (CTRL). The released dye was captured by a cation exchanger resin Dowex (10–15 mg per well). The absorbance (OD) of residual dye was measured at a wavelength of 595 nm using the Infinite 200 PRO system (Tecan). To investigate the capacity of liposomes to inhibit HBL-induced activation of the inflammasome, recombinant HBL (5 nM) was left untreated or treated with liposomes (7 mM) for 1 hr, prior to addition to LPS-primed BMDMs.

## Immunoblotting Analysis

For caspase-1 immunoblotting, BMDMs and supernatant were lysed in RIPA buffer and sample loading buffer containing SDS and 100 mM DTT. For immunoblotting of pIkB, IkB, pERK, ERK, NLRP3 and GAPDH, the supernatant was removed and BMDMs washed once with PBS, followed by lysis in RIPA buffer and sample loading buffer containing SDS and 100 mM DTT. Proteins were separated on 8–12% polyacrylamide gels. Following electrophoretic transfer of proteins onto PVDF membranes (IPVH00010, Millipore),

membranes were blocked in 5% skim milk and incubated overnight with primary antibodies against caspase-1 (1:1,000 dilution, #AG-20B-0042, Adipogen), pIkB (1:1,000 dilution, #2859, Cell Signaling Technologies), IkB (1:1,000 dilution, #9242, Cell Signaling Technologies), pERK (1:1,000 dilution, #9101, Cell Signaling Technologies), ERK (1:1,000 dilution, #9102, Cell Signaling Technologies), NLRP3 (1:1,000 dilution, #AG-20B-0014, Adipogen), GAPDH (1:10,000 dilution, #5174, Cell Signaling Technologies), or Pan-cadherin (1:1,000 dilution, #4068, Cell Signaling Technologies), Gasdermin D (1:1,000 dilution, #ab209845, Abcam), or IL-1β (1:1,000 dilution, #RDSAF401NA, R&D Systems). PVDF membranes were then incubated with HRP-conjugated secondary antibody for 1 hr and proteins were visualized using the Super Signal Femto substrate (34095, ThermoFisher Scientific) and the ChemiDoc™Touch Imaging System (BioRad).

For detection of toxin components, 300 μl of the supernatant of *B. cereus* were mixed with 100 μl of sample loading buffer. Primary antibodies against HBL components B, $L_1$ and $L_2$ (1:1,000 dilution)[40], or against NHE-B (1:1,000 dilution)[75] were used. Silver staining was performed for total protein loading controls in accordance with the manufacturer's instructions (24612, Thermo Scientific).

## Immunofluorescence Staining

For visualization of inflammasomes, untreated or treated BMDMs were washed three times with PBS and fixed with 4% paraformaldehyde at room temperature for 15 min, followed by blocking in 10% normal goat serum (005000121, Jackson ImmunoResearch) supplemented with 0.1% saponin (47036, Sigma) for 1 hr. Cells were incubated with a rabbit anti-ASC antibody (1:500 dilution, clone AL177, AG-25B-0006-C100, AdipoGen) overnight at 4 °C. An anti-rabbit secondary Rhodamine red antibody (111295144, Jackson ImmunoResearch) was used. Cells were counterstained in DAPI mounting medium (H-1200, Vecta Labs). Inflammasome specks and BMDMs were visualized, counted, and imaged using a Leica SP5 confocal microscope. For visualization of HBL and cell membrane, BMDMs were stimulated with HBL component B (5 μg/ml) for 1 hr, washed three times with PBS and fixed with 4% paraformaldehyde at room temperature for 15 min, followed by blocking in 1% BSA in PBS for 1 hr. Cells were incubated with a mouse anti-HBL-B antibody (1:200 dilution in 1% BSA)[40] and a rat FITC-conjugated anti-CD11b antibody (1:200 dilution in 1% BSA, 101205, BioLegend) overnight at 4 °C. PBS containing 0.05% Tween-20 was used to wash between incubation steps. An anti-mouse secondary Rhodamine red antibody (115295146, Jackson ImmunoResearch) was used. BMDMs were analysed using a Leica SP5 confocal microscope.

## Immunological Lateral Flow Tests

The antibody-based assay Duopath Cereus Enterotoxins (1041460001, Merck) detects the presence of the HBL component $L_2$ and NHE-B in the supernatant of *B. cereus*. The supernatant of *B. cereus* was applied to the Duopath cassette according to the manufacturer's instructions. Sterile LB broth and filter-sterilized supernatant from an overnight culture of *S.* Typhimurium were used as negative controls.

### Cryo-Electron Microscopy

Liposomes left untreated or treated with recombinant HBL (0.5 μM) for 1 hr were applied on a holey carbon 400 mesh grid and left to adhere for 30 s. Grids were then blotted for 10 s to remove excess liposomes before plunge frozen using liquid ethane surrounded by a bath of liquid nitrogen. Samples were visualized under Hitachi 7100 TEM at 100kv with a Cryo-TEM holder.

### Scanning Electron Microscopy

BMDMs were washed with PBS and post-fixed with 2.5% glutaraldehyde in 0.1 M phosphate buffer overnight and further washed with PBS. Cells were fixed in 1% osmium tetroxide in double distilled water for 1 hr and dehydrated in a series of alcohol. Dehydrated samples were dried using liquid carbon dioxide using critical point drying. Samples were then sputter-coated with platinum (3 nm thickness) at 15 mA for 2 min using the EMI TECH K550 Sputter coater and visualized under a Zeiss UltraPlus Field emission scanning electron microscope at 5 kV.

### Transmission Electron Microscopy

BMDMs were washed with PBS and post-fixed with 2.5% glutaraldehyde in 0.1 M phosphate buffer overnight and further washed with PBS. Cells were fixed in 1% osmium tetroxide in double distilled water for 1 hr and dehydrated in a series of alcohol, and embedded in LR white resin (C023, ProSciTech). Samples were polymerized in a 60 °C oven overnight. Thin sections were cut at 80 nm and viewed using a Hitachi HA7100 transmission electron microscope at 100 kV.

### Separation of Membrane and Cytosolic Compartments

BMDMs were stimulated with either purified recombinant HBL protein (5 nM) or the supernatant of *B. cereus* (50 μl) for 45 min, washed three times with PBS followed by separation of membrane and cytosolic fractions using the Mem-PER Plus Membrane Protein Extraction Kit according to the manufacturer's instructions (89842, Thermo Scientific).

### Lactate Dehydrogenase Assay

Levels of lactate dehydrogenase released by cells were determined using the CytoTox 96 Non-Radioactive Cytotoxicity Assay according to the manufacturer's instructions (G1780, Promega).

### IncuCyte Analysis

To track the viability of BMDMs in response to HBL, BMDMs were stimulated with a high concentration of HBL (0.5 μM) or a low concentration of HBL (5 nM) in presence of the SYTOX Green nuclear stain that penetrates compromised membranes (1 μM; S7020; Life Technologies). Cells were monitored over 3 hr using the IncuCyte Zoom "in-incubator" imaging system (Essen Biosciences).

### Real Time qRT-PCR Analysis

RNA was extracted from BMDMs using TRIzol (15596018, ThermoFisher Scientific) and from bacteria using the TRIzol Max Bacterial RNA Isolation kit (16096040, ThermoFisher). The isolated RNA was converted into cDNA using the High-Capacity cDNA Reverse Transcription Kit (4368813, ThermoFisher). Real-time qPCR was performed on an ABI StepOnePlus System PCR instrument with SYBR Green Real-Time PCR Master Mixes (4364346, ThermoFisher). Real time qRT-PCR sequences can be found in Supplementary Table 2.

### Cytokine Analysis

Cytokine levels were determined using a multiplex ELISA (MCYTOMAG-70K, EMD Millipore) or IL-18 ELISA (EK-0048, ELISAkit.com) according to the manufacturers' instructions.

### Amino Acid Sequence Analysis

Putative transmembrane regions in individual components of HBL were predicted using the software Membrane Protein Explorer server, also known as MPEx[77]. Helical wheel diagrams were constructed using the HELIQUEST server[78].

### Animal Infection

*B. cereus* strains were grown as described above. For survival analysis, 8-week-old mice were injected via an intraperitoneal (i.p.) route with $5 \times 10^6$ colony-forming units (CFUs) of *B. cereus*. For cytokine measurement in the serum, mice were injected, via an i.p. route, with $7.5 \times 10^6$ CFUs of an overnight culture of *B. cereus* or 200 μl of filter-sterilized supernatant of *B. cereus*. For cytokine measurement in the peritoneal fluid, mice were injected, via an i.p. route, with $7.5 \times 10^6$ CFUs of *B. cereus*. The peritoneal fluid and serum were collected after 3–20 hr for analysis by ELISA. To investigate the effects of MCC950 [34], mice were injected, via an i.p. route, with 50 mg/kg of MCC950 dissolved in PBS or with vehicle control PBS. 1 hr later, mice were injected, via an i.p. route, with $5 \times 10^6$ CFUs of *B. cereus* along with a second dose of 50 mg/kg of MCC950 or a second dose of PBS.

### Statistical Analysis

The GraphPad Prism 6.0 software was used for data analysis. Data are shown as mean ± s.e.m. Statistical significance was determined by *t* tests (two-tailed) for two groups or One-way ANOVA (with Dunnett's or Tukey's multiple comparisons tests) for three or more groups. Survival curves were compared using the log-rank test. $P<0.05$ was considered statistically significant. In this study, no statistical methods were used to predetermine the sample size. The experiments were not randomized, and the investigators were not blinded to allocation during the experiments and outcome assessment.

## Supplementary Material

Refer to Web version on PubMed Central for supplementary material.

## ACKNOWLEDGEMENTS

We would like to thank Dr. V.M. Dixit (Genentech, USA), Dr. K. Schroder (Institute of Molecular Bioscience, Australia), Dr. P. Broz (University of Lausanne, Switzerland), Dr. J. Ng (Westmead Hospital, Australia), Mrs A. Rice (The Canberra Hospital, Australia), and Mr. J. Bates (Department of Health Queensland, Australia) for reagents. We thank Dr. B. Quah (ANU, Australia), Ms. Cathy Gillespie (ANU, Australia), Dr. I. Sastalla (National Institutes of Health, USA), Dr. M. Rug (Centre for Advanced Microscopy, ANU, Australia), Ms. J. Lee (Centre for Advanced Microscopy, ANU, Australia), Dr. C. O'Brien (The Canberra Hospital, Australia), and Dr. D. Gordon (ANU, Australia) for assistance. A.M. is supported by a John Curtin School of Medical Research International PhD scholarship. S.H.L. is supported in part by the Intramural Program of the National Institute of Allergy and Infectious Diseases, NIH, USA. N.O.K. is supported by a Career Development Fellowship from the Cancer Institute NSW (15/CDF/1-11). S.M.M. is supported by the Australian National University, The Gretel and Gordon Bootes Medical Research Foundation, and the National Health and Medical Research Council of Australia under Project Grants (APP1141504 and APP1146864) and the R.G. Menzies Early Career Fellowship (APP1091544).

## REFERENCES

1. Schroder K. & Tschopp J. The inflammasomes. Cell 140, 821–832 (2010).
2. Lamkanfi M. & Dixit VM Mechanisms and functions of inflammasomes. Cell 157, 1013–1022 (2014).
3. Rathinam VA & Fitzgerald KA Inflammasome Complexes: Emerging Mechanisms and Effector Functions. Cell 165, 792–800 (2016).
4. Latz E, Xiao TS & Stutz A. Activation and regulation of the inflammasomes. Nat Rev Immunol 13, 397–411 (2013).
5. Man SM & Kanneganti TD Converging roles of caspases in inflammasome activation, cell death and innate immunity. Nat Rev Immunol 16, 7–21 (2016).
6. Man SM, et al. IRGB10 Liberates Bacterial Ligands for Sensing by the AIM2 and Caspase-11-NLRP3 Inflammasomes. Cell 167, 382–396.e317 (2016).
7. Man SM, et al. The transcription factor IRF1 and guanylate-binding proteins target activation of the AIM2 inflammasome by Francisella infection. Nat Immunol 16, 467–475 (2015).
8. Meunier E, et al. Caspase-11 activation requires lysis of pathogen-containing vacuoles by IFN-induced GTPases. Nature 509, 366–370 (2014).
9. Meunier E, et al. Guanylate-binding proteins promote activation of the AIM2 inflammasome during infection with Francisella novicida. Nat Immunol 16, 476–484 (2015).
10. Mariathasan S, et al. Differential activation of the inflammasome by caspase-1 adaptors ASC and Ipaf. Nature 430, 213–218 (2004).
11. Kofoed EM & Vance RE Innate immune recognition of bacterial ligands by NAIPs determines inflammasome specificity. Nature 477, 592–595 (2011).
12. Zhao Y, et al. The NLRC4 inflammasome receptors for bacterial flagellin and type III secretion apparatus. Nature 477, 596–600 (2011).
13. Miao EA, et al. Cytoplasmic flagellin activates caspase-1 and secretion of interleukin 1beta via Ipaf. Nat Immunol 7, 569–575 (2006).
14. Franchi L, et al. Cytosolic flagellin requires Ipaf for activation of caspase-1 and interleukin 1beta in salmonella-infected macrophages. Nat Immunol 7, 576–582 (2006).
15. Amer A, et al. Regulation of Legionella phagosome maturation and infection through flagellin and host Ipaf. J Biol Chem 281, 35217–35223 (2006).
16. Liu S, Moayeri M. & Leppla SH Anthrax lethal and edema toxins in anthrax pathogenesis. Trends Microbiol 22, 317–325 (2014).
17. Dal Peraro M. & van der Goot FG Pore-forming toxins: ancient, but never really out of fashion. Nat Rev Microbiol 14, 77–92 (2016).
18. Mariathasan S, et al. Cryopyrin activates the inflammasome in response to toxins and ATP. Nature 440, 228–232 (2006).
19. Muñoz-Planillo R, Franchi L, Miller LS & Núñez G. A Critical Role for Hemolysins and Bacterial Lipoproteins in Staphylococcus aureus-Induced Activation of the Nlrp3 Inflammasome. Journal of immunology (Baltimore, Md. : 1950) 183, 3942–3948 (2009).

20. Craven RR, et al. Staphylococcus aureus alpha-hemolysin activates the NLRP3-inflammasome in human and mouse monocytic cells. PLoS One 4, e7446 (2009).
21. Kebaier C, et al. Staphylococcus aureus alpha-hemolysin mediates virulence in a murine model of severe pneumonia through activation of the NLRP3 inflammasome. J Infect Dis 205, 807–817 (2012).
22. Zhang X, et al. Enterohemorrhagic Escherichia coli specific enterohemolysin induced IL-1beta in human macrophages and EHEC-induced IL-1beta required activation of NLRP3 inflammasome. PLoS One 7, e50288 (2012).
23. Schaale K, et al. Strain- and host species-specific inflammasome activation, IL-1β release, and cell death in macrophages infected with uropathogenic Escherichia coli. Mucosal Immunology 9, 124 (2015).
24. Costa A, et al. Activation of the NLRP3 inflammasome by group B streptococci. J Immunol 188, 1953–1960 (2012).
25. Whidbey C, et al. A streptococcal lipid toxin induces membrane permeabilization and pyroptosis leading to fetal injury. EMBO Mol Med 7, 488–505 (2015).
26. Gupta R, et al. RNA and beta-hemolysin of group B Streptococcus induce interleukin-1beta (IL-1beta) by activating NLRP3 inflammasomes in mouse macrophages. J Biol Chem 289, 13701–13705 (2014).
27. Harder J, et al. Activation of the Nlrp3 inflammasome by Streptococcus pyogenes requires streptolysin O and NF-kappa B activation but proceeds independently of TLR signaling and P2X7 receptor. J Immunol 183, 5823–5829 (2009).
28. Keyel PA, Roth R, Yokoyama WM, Heuser JE & Salter RD Reduction of streptolysin O (SLO) pore-forming activity enhances inflammasome activation. Toxins (Basel) 5, 1105–1118 (2013).
29. Ozoren N, et al. Distinct roles of TLR2 and the adaptor ASC in IL-1beta/IL-18 secretion in response to Listeria monocytogenes. J Immunol 176, 4337–4342 (2006).
30. Hamon MA & Cossart P. K+ efflux is required for histone H3 dephosphorylation by Listeria monocytogenes listeriolysin O and other pore-forming toxins. Infect Immun 79, 2839–2846 (2011).
31. Toma C, et al. Pathogenic Vibrio activate NLRP3 inflammasome via cytotoxins and TLR/nucleotide-binding oligomerization domain-mediated NF-kappa B signaling. J Immunol 184, 5287–5297 (2010).
32. Higa N, et al. Vibrio parahaemolyticus effector proteins suppress inflammasome activation by interfering with host autophagy signaling. PLoS Pathog 9, e1003142 (2013).
33. Song L, et al. A critical role for hemolysin in Vibrio fluvialis-induced IL-1beta secretion mediated by the NLRP3 inflammasome in macrophages. Front Microbiol 6, 510 (2015).
34. Coll RC, et al. A small-molecule inhibitor of the NLRP3 inflammasome for the treatment of inflammatory diseases. Nat Med 21, 248–255 (2015).
35. Man SM & Kanneganti TD Regulation of inflammasome activation. Immunol Rev 265, 6–21 (2015).
36. Bottone EJ Bacillus cereus, a volatile human pathogen. Clin Microbiol Rev 23, 382–398 (2010).
37. Beecher DJ & Wong AC Improved purification and characterization of hemolysin BL, a hemolytic dermonecrotic vascular permeability factor from Bacillus cereus. Infect Immun 62, 980–986 (1994).
38. Heinrichs JH, Beecher DJ, MacMillan JD & Zilinskas BA Molecular cloning and characterization of the hblA gene encoding the B component of hemolysin BL from Bacillus cereus. J Bacteriol 175, 6760–6766 (1993).
39. Ryan PA, Macmillan JD & Zilinskas BA Molecular cloning and characterization of the genes encoding the L1 and L2 components of hemolysin BL from Bacillus cereus. J Bacteriol 179, 2551–2556 (1997).
40. Sastalla I, et al. The Bacillus cereus Hbl and Nhe tripartite enterotoxin components assemble sequentially on the surface of target cells and are not interchangeable. PLoS One 8, e76955 (2013).
41. Lund T, De Buyser ML & Granum PE A new cytotoxin from Bacillus cereus that may cause necrotic enteritis. Mol Microbiol 38, 254–261 (2000).

42. Beecher DJ & Wong AC Tripartite hemolysin BL from Bacillus cereus. Hemolytic analysis of component interactions and a model for its characteristic paradoxical zone phenomenon. J Biol Chem 272, 233–239 (1997).
43. Levinsohn JL, et al. Anthrax lethal factor cleavage of Nlrp1 is required for activation of the inflammasome. PLoS Pathog 8, e1002638 (2012).
44. Hellmich KA, et al. Anthrax lethal factor cleaves mouse nlrp1b in both toxin-sensitive and toxin-resistant macrophages. PLoS One 7, e49741 (2012).
45. Moayeri M, et al. Inflammasome sensor Nlrp1b-dependent resistance to anthrax is mediated by caspase-1, IL-1 signaling and neutrophil recruitment. PLoS Pathog 6, e1001222 (2010).
46. Man SM, et al. Actin polymerization as a key innate immune effector mechanism to control Salmonella infection. Proc Natl Acad Sci U S A 111, 17588–17593 (2014).
47. Madegowda M, Eswaramoorthy S, Burley SK & Swaminathan S. X-ray crystal structure of the B component of Hemolysin BL from Bacillus cereus. Proteins 71, 534–540 (2008).
48. Yohannan S, Faham S, Yang D, Whitelegge JP & Bowie JU The evolution of transmembrane helix kinks and the structural diversity of G protein-coupled receptors. Proc Natl Acad Sci U S A 101, 959–963 (2004).
49. Cordes FS, Bright JN & Sansom MS Proline-induced distortions of transmembrane helices. J Mol Biol 323, 951–960 (2002).
50. Jin T, et al. The (beta)gamma subunits of G proteins gate a K(+) channel by pivoted bending of a transmembrane segment. Mol Cell 10, 469–481 (2002).
51. Tieleman DP, Shrivastava IH, Ulmschneider MR & Sansom MS Proline-induced hinges in transmembrane helices: possible roles in ion channel gating. Proteins 44, 63–72 (2001).
52. Miao EA, et al. Caspase-1-induced pyroptosis is an innate immune effector mechanism against intracellular bacteria. Nat Immunol 11, 1136–1142 (2010).
53. Jorgensen I, Zhang Y, Krantz BA & Miao EA Pyroptosis triggers pore-induced intracellular traps (PITs) that capture bacteria and lead to their clearance by efferocytosis. J Exp Med 213, 2113–2128 (2016).
54. Hayward JA, Mathur A, Ngo C. & Man SM Cytosolic Recognition of Microbes and Pathogens: Inflammasomes in Action. Microbiology and Molecular Biology Reviews 82(2018).
55. Perregaux D. & Gabel CA Interleukin-1 beta maturation and release in response to ATP and nigericin. Evidence that potassium depletion mediated by these agents is a necessary and common feature of their activity. J Biol Chem 269, 15195–15203 (1994).
56. Petrilli V, et al. Activation of the NALP3 inflammasome is triggered by low intracellular potassium concentration. Cell Death Differ 14, 1583–1589 (2007).
57. Munoz-Planillo R, et al. K(+) efflux is the common trigger of NLRP3 inflammasome activation by bacterial toxins and particulate matter. Immunity 38, 1142–1153 (2013).
58. Henry T, Brotcke A, Weiss DS, Thompson LJ & Monack DM Type I interferon signaling is required for activation of the inflammasome during Francisella infection. J Exp Med 204, 987–994 (2007).
59. Hara H, et al. Dependency of caspase-1 activation induced in macrophages by Listeria monocytogenes on cytolysin, listeriolysin O, after evasion from phagosome into the cytoplasm. J Immunol 180, 7859–7868 (2008).
60. Ehling-Schulz M, Fricker M. & Scherer S. Bacillus cereus, the causative agent of an emetic type of food-borne illness. Mol Nutr Food Res 48, 479–487 (2004).
61. Man SM, et al. Differential roles of caspase-1 and caspase-11 in infection and inflammation. Sci Rep 7, 45126 (2017).
62. Tate MD, et al. Reassessing the role of the NLRP3 inflammasome during pathogenic influenza A virus infection via temporal inhibition. Sci Rep 6, 27912 (2016).
63. Primiano MJ, et al. Efficacy and Pharmacology of the NLRP3 Inflammasome Inhibitor CP-456,773 (CRID3) in Murine Models of Dermal and Pulmonary Inflammation. J Immunol 197, 2421–2433 (2016).
64. Mridha AR, et al. NLRP3 inflammasome blockade reduces liver inflammation and fibrosis in experimental NASH in mice. J Hepatol 66, 1037–1046 (2017).

65. Chen W, et al. Specific inhibition of NLRP3 in chikungunya disease reveals a role for inflammasomes in alphavirus-induced inflammation. Nat Microbiol 2, 1435–1445 (2017).
66. Moayeri M, et al. Small-molecule inhibitors of lethal factor protease activity protect against anthrax infection. Antimicrob Agents Chemother 57, 4139–4145 (2013).
67. Leysath CE, et al. Mouse monoclonal antibodies to anthrax edema factor protect against infection. Infect Immun 79, 4609–4616 (2011).
68. Lund T. & Granum PE Characterisation of a non-haemolytic enterotoxin complex from Bacillus cereus isolated after a foodborne outbreak. FEMS Microbiol Lett 141, 151–156 (1996).
69. Ganash M, et al. Structure of the NheA component of the Nhe toxin from Bacillus cereus: implications for function. PLoS One 8, e74748 (2013).
70. Haug TM, et al. Formation of very large conductance channels by Bacillus cereus Nhe in Vero and GH(4) cells identifies NheA + B as the inherent pore-forming structure. J Membr Biol 237, 1–11 (2010).
71. Jones JW, et al. Absent in melanoma 2 is required for innate immune recognition of Francisella tularensis. Proc Natl Acad Sci U S A 107, 9771–9776 (2010).
72. Kuida K, et al. Altered cytokine export and apoptosis in mice deficient in interleukin-1 beta converting enzyme. Science 267, 2000–2003 (1995).
73. Wang S, et al. Murine caspase-11, an ICE-interacting protease, is essential for the activation of ICE. Cell 92, 501–509 (1998).
74. Kovarova M, et al. NLRP1-dependent pyroptosis leads to acute lung injury and morbidity in mice. J Immunol 189, 2006–2016 (2012).
75. Dietrich R, Moravek M, Burk C, Granum PE & Martlbauer E. Production and characterization of antibodies against each of the three subunits of the Bacillus cereus nonhemolytic enterotoxin complex. Appl Environ Microbiol 71, 8214–8220 (2005).
76. van Meer G, Voelker DR & Feigenson GW Membrane lipids: where they are and how they behave. Nat Rev Mol Cell Biol 9, 112–124 (2008).
77. Snider C, Jayasinghe S, Hristova K. & White SH MPEx: a tool for exploring membrane proteins. Protein Sci 18, 2624–2628 (2009).
78. Gautier R, Douguet D, Antonny B. & Drin G. HELIQUEST: a web server to screen sequences with specific alpha-helical properties. Bioinformatics 24, 2101–2102 (2008).

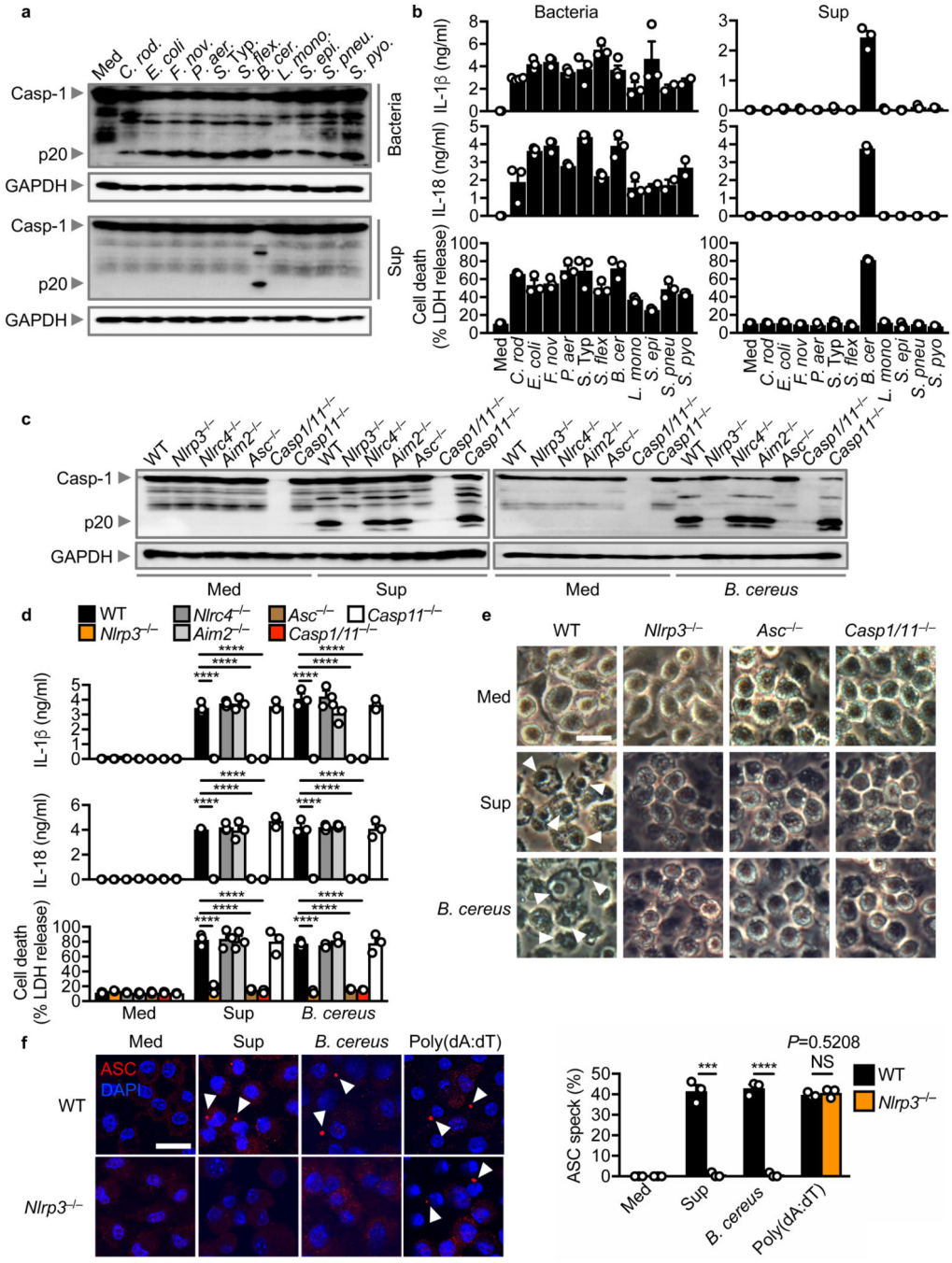


**Fig. 1 |. A secreted factor of *B. cereus* activates the NLRP3 inflammasome.**

(**a**) Immunoblot analysis of pro-caspase-1 (Casp-1) and the caspase-1 subunit p20 (p20) and GAPDH (loading control) in wild-type (WT) BMDMs left untreated (medium alone [Med]) or assessed at various times after infection with *Citrobacter rodentium*, *Escherichia coli*, *Francisella novicida*, *Pseudomonas aeruginosa*, *Salmonella enterica* serovar Typhimurium, *Shigella flexneri*, *Bacillus cereus*, *Listeria monocytogenes*, *Staphylococcus epidermidis*, *Streptococcus pneumoniae*, *Streptococcus pyogenes* (top) or after stimulation with the supernatant (Sup) of the corresponding bacteria (bottom). (**b**) Release of IL-1β (top) and

IL-18 (middle), and death (bottom) of BMDMs after treatment as in (a). (**c**) Immunoblot analysis of caspase-1 and GAPDH in WT or mutant BMDMs left untreated or assessed 2 hr after stimulation with the supernatant of *B. cereus* (Sup) (left) or 3 hr after infection with *B. cereus* (MOI, 5; right). *B. cereus* ATCC 14579 is used throughout unless otherwise stated. (**d**) Release of IL-1β (top) and IL-18 (middle), and death (bottom) of BMDMs after treatment as in (c). (**e**) Microscopy analysis of the death of BMDMs after treatment as in (c). (**f**) Confocal microscopy analysis of ASC (red) in WT or *Nlrp3*$^{-/-}$ BMDMs left untreated or assessed 2 hr after stimulation with the supernatant of *B. cereus* (Sup), 3 hr after infection with *B. cereus* (MOI, 5), or 5 hr after transfection with poly(dA:dT) (left). Quantification of the prevalence of ASC inflammasome speck (right). At least 200 BMDMs from each genotype were analysed. Scale bars, 20 μm (e and f). Arrowheads indicate dead cells (e) or inflammasome specks (f). Each symbol represents an independent experiment (b, d and f). NS, not statistically significant, ***$P < 0.001$ and ****$P < 0.0001$ (one-way analysis of variance [ANOVA] with Dunnett's multiple-comparisons test [d]; two-tailed *t*-test [f]). Data are representative of at least two independent experiments (n=2–3 in b and n=3 in a, c-f; mean and s.e,m. in b, d and f).

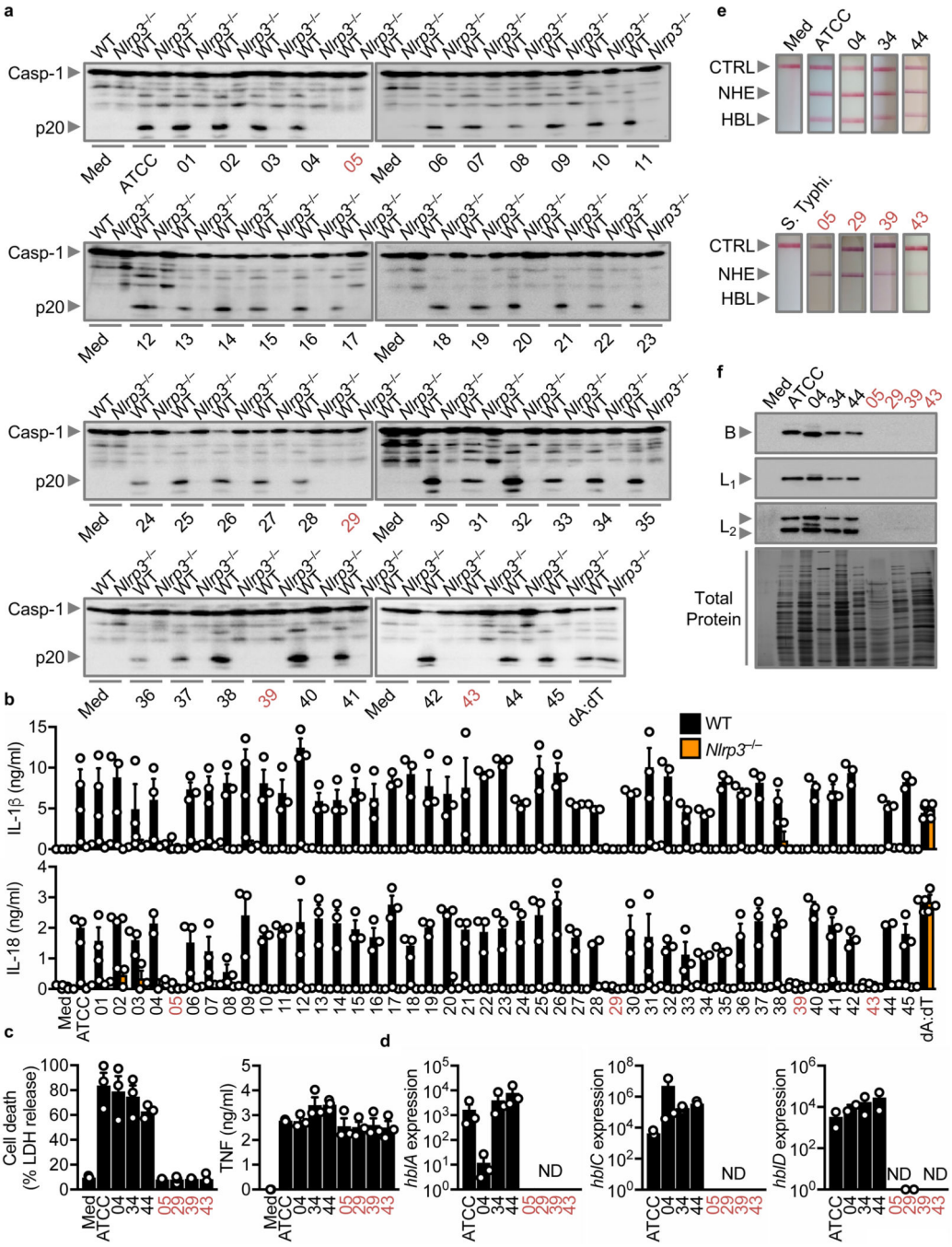


**Fig. 2 |. The inflammasome-activating factor is highly prevalent in *B. cereus* isolates and is associated with isolates expressing HBL.**

(**a**) Immunoblot analysis of caspase-1 of LPS-primed WT or *Nlrp3*$^{-/-}$ BMDMs left untreated (Med) or assessed at various times after stimulation with supernatant of overnight cultures of 46 *B. cereus* strains or 5 hr after transfection with poly(dA:dT). The list of strains used is available in Table S1. ATCC refers to ATCC 14579. (**b**) Release of IL-1β (top) and IL-18 (bottom) of LPS-primed WT or *Nlrp3*$^{-/-}$ BMDMs after treatment as in (a). (**c**) Cell death and release of TNF of LPS-primed WT BMDMs after treatment as in (a). (**d**) Real-time

quantitative RT-PCR analysis of the gene encoding the HBL components B (*hblA*), $L_2$ (*hblC*), and $L_1$ (*hblD*) of overnight culture of *B. cereus*, presented relative to that of the gene encoding 16S rRNA. (**e**) Immunological lateral flow tests (Duopath) of NHE and HBL using LB broth (Med) or supernatant of overnight cultures of *B. cereus* isolates or *S.* Typhimurium (*S.* Typhi). (**f**) Immunoblot analysis of the HBL components B, $L_1$, and $L_2$ in the supernatant of overnight cultures of *B. cereus* and silver stain of the total protein. Numerical IDs of *B. cereus* strains unable to activate caspase-1 are colorized (a-f). CTRL, control (e), Each symbol represents an independent experiment (b-d). NS, not statistically significant, ND, not detected, (two-tailed *t*-test; B). Data are representative of at least two independent experiments (n=3 in a, c-f, n=2–3 in b; mean and s.e.m. in b-d).

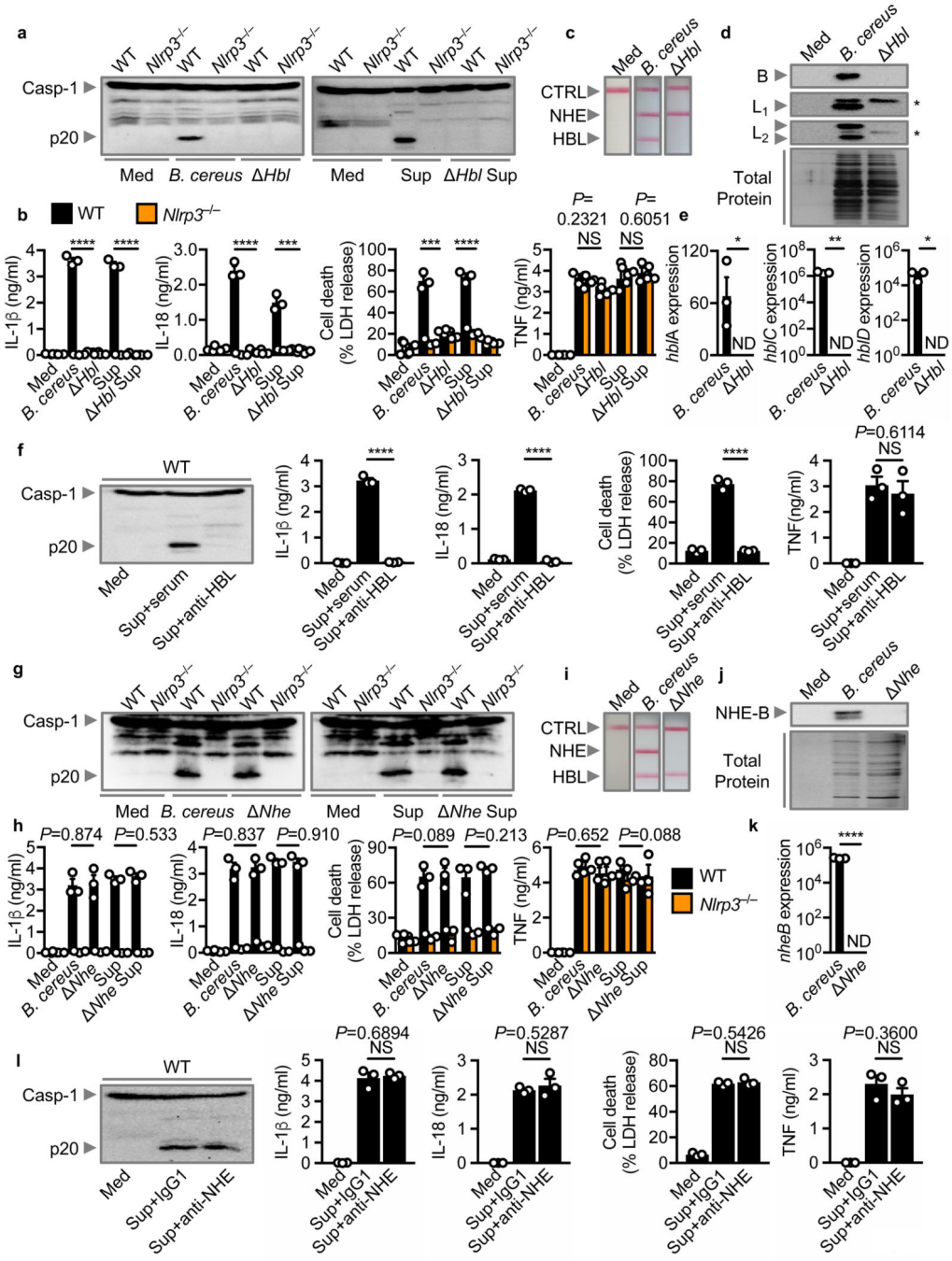


**Fig. 3 |. HBL triggers activation of the NLRP3 inflammasome.**

(**a**) Immunoblot analysis of caspase-1 of unprimed WT or *Nlrp3*$^{-/-}$ BMDMs left untreated (Med) or assessed 3 hr after infection with *B. cereus* ATCC 10876 (MOI, 5) or its isogenic mutant lacking HBL (Δ*Hbl*; [MOI, 5]) (left). Immunoblot analysis of caspase-1 of LPS-primed WT or *Nlrp3*$^{-/-}$ BMDMs left untreated or assessed 2 hr after stimulation with the supernatant of *B. cereus* (Sup) or Δ*Hbl B. cereus* supernatant (Δ*Hbl* Sup) (right). (**b**) Release of IL-1β (left) and IL-18 (middle-left), death (middle-right), and release of TNF (right) of WT or *Nlrp3*$^{-/-}$ BMDMs after treatment as in (a). (**c**) Immunological lateral flow tests

(Duopath) of NHE and HBL using LB broth (Med) or supernatant of overnight cultures of *B. cereus* or Δ*Hbl B. cereus*. (**d**) Immunoblot analysis of the HBL components B, $L_1$ and $L_2$ in the supernatant of overnight cultures of *B. cereus* or Δ*Hbl B. cereus*, and silver stain of the total protein. (**e**) Real-time quantitative RT-PCR analysis of the gene encoding *hblA*, *hblC*, and *hblD* in overnight cultures of *B. cereus* or Δ*Hbl B. cereus*, presented relative to that of the gene encoding 16S rRNA. (**f**) Immunoblot analysis of caspase-1 (left), the release of IL-1β (middle-left) and IL-18 (middle), death (middle-right), and release of TNF (right) of LPS-primed WT BMDMs left untreated or assessed 2 hr after stimulation with the supernatant of *B. cereus* (Sup) incubated with mouse serum (serum) or supernatant incubated with anti-HBL antibodies (anti-HBL). (**g-l**) A similar analysis as above was conducted using *B. cereus* F837/76 or its isogenic mutant lacking NHE (Δ*Nhe*). Asterisks in (d) indicate non-specific bands. CTRL, control (c and i), Each symbol represents an independent experiment (b, e, f, h, k and l). NS, not statistically significant, ND, not detected, $*P < 0.05$, $**P < 0.01$, $***P < 0.001$ and $****P < 0.0001$ (two-tailed *t*-test [b, e, f, h, k, l]). Data are representative of three independent experiments (n=3 in a-l; mean and s.e.m. in b, e, f, h, k and l).

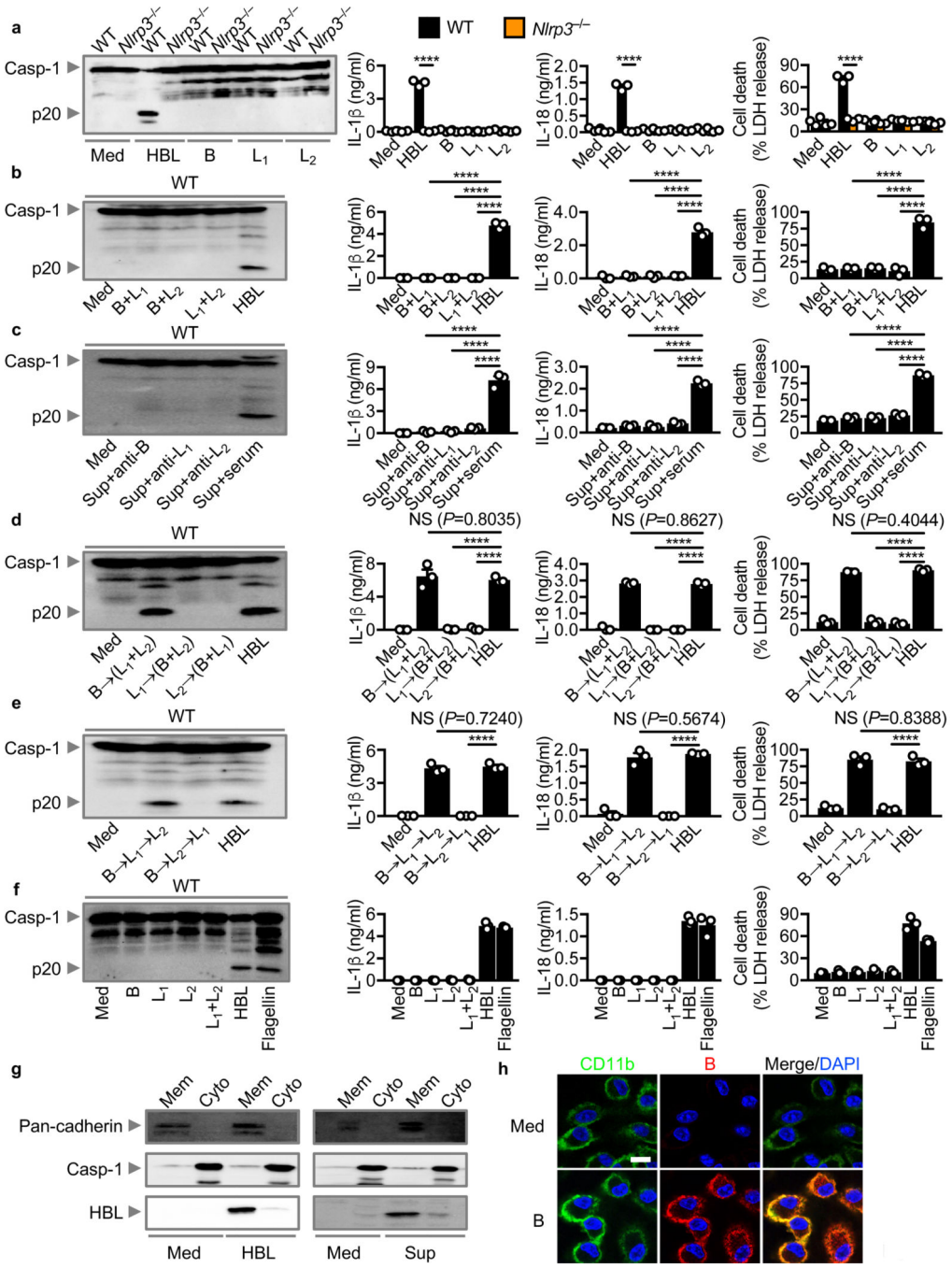


**Fig. 4 |. Recombinant HBL components assemble sequentially to induce activation of the NLRP3 inflammasome.**

(**a**) Immunoblot analysis of caspase-1 (left), the release of IL-1β (middle-left) and IL-18 (middle-right), and death (right) of LPS-primed WT or *Nlrp3*$^{-/-}$ BMDMs left untreated (Med) or assessed 3 hr after stimulation with recombinant HBL or individual HBL components B, $L_1$ or $L_2$. (**b**) Immunoblot analysis of caspase-1 (left), the release of IL-1β (middle-left) and IL-18 (middle-right), and death (right) of LPS-primed WT BMDMs left untreated or assessed 3 hr after stimulation with two components of HBL. (**c**) Immunoblot

analysis of caspase-1 (left), the release of IL-1β (middle-left) and IL-18 (middle-right), and death (right) of LPS-primed WT BMDMs left untreated or assessed 2 hr after stimulation with the supernatant of *B. cereus* (Sup) incubated with an antibody against either B, $L_1$ or $L_2$, or with mouse serum (serum). (**d**) Immunoblot analysis of caspase-1 (left), the release of IL-1β (middle-left) and IL-18 (middle-right), and death (right) of LPS-primed WT BMDMs left untreated or assessed 3 hr after treatment with either B→($L_1$+$L_2$) or $L_1$→(B+$L_2$) or $L_2$→(B+$L_1$). (**e**) Immunoblot analysis of caspase-1 (left), the release of IL-1β (middle-left) and IL-18 (middle-right), and death (right) of LPS-primed WT BMDMs left untreated or assessed 3 hr after treatment with either B→$L_1$→$L_2$ or B→$L_2$→$L_1$. (**f**) Immunoblot analysis of caspase-1 (left), the release of IL-1β (middle-left) and IL-18 (middle-right), and death (right) of LPS-primed WT BMDMs left untreated or assessed 2 hr after transfection with one or two components of HBL, or after stimulation with recombinant HBL, or after transfection with flagellin of *S.* Typhimurium. (**g**) Immunoblot analysis of pan-cadherin, caspase-1 and HBL of unprimed WT BMDMs left untreated (Med) or assessed 1 hr after stimulation with recombinant HBL or the supernatant of *B. cereus* (Sup). Mem, membrane fraction; Cyto, cytosolic fraction. (**h**) Confocal microscopy analysis of CD11b (green) and HBL-B (red) in unprimed WT BMDMs left untreated or assessed 1 hr after stimulation with the individual component HBL-B. Scale bar, 10 μm (h); Each symbol represents an independent experiment (a-f). NS, not statistically significant, ****$P < 0.0001$ (two-tailed *t*-test [a] or one-way analysis of variance [ANOVA] with Dunnett's multiple-comparisons test [b-e]). Data are representative of three independent experiments (n=3 in a-h; mean and s.e.m. in a-f).

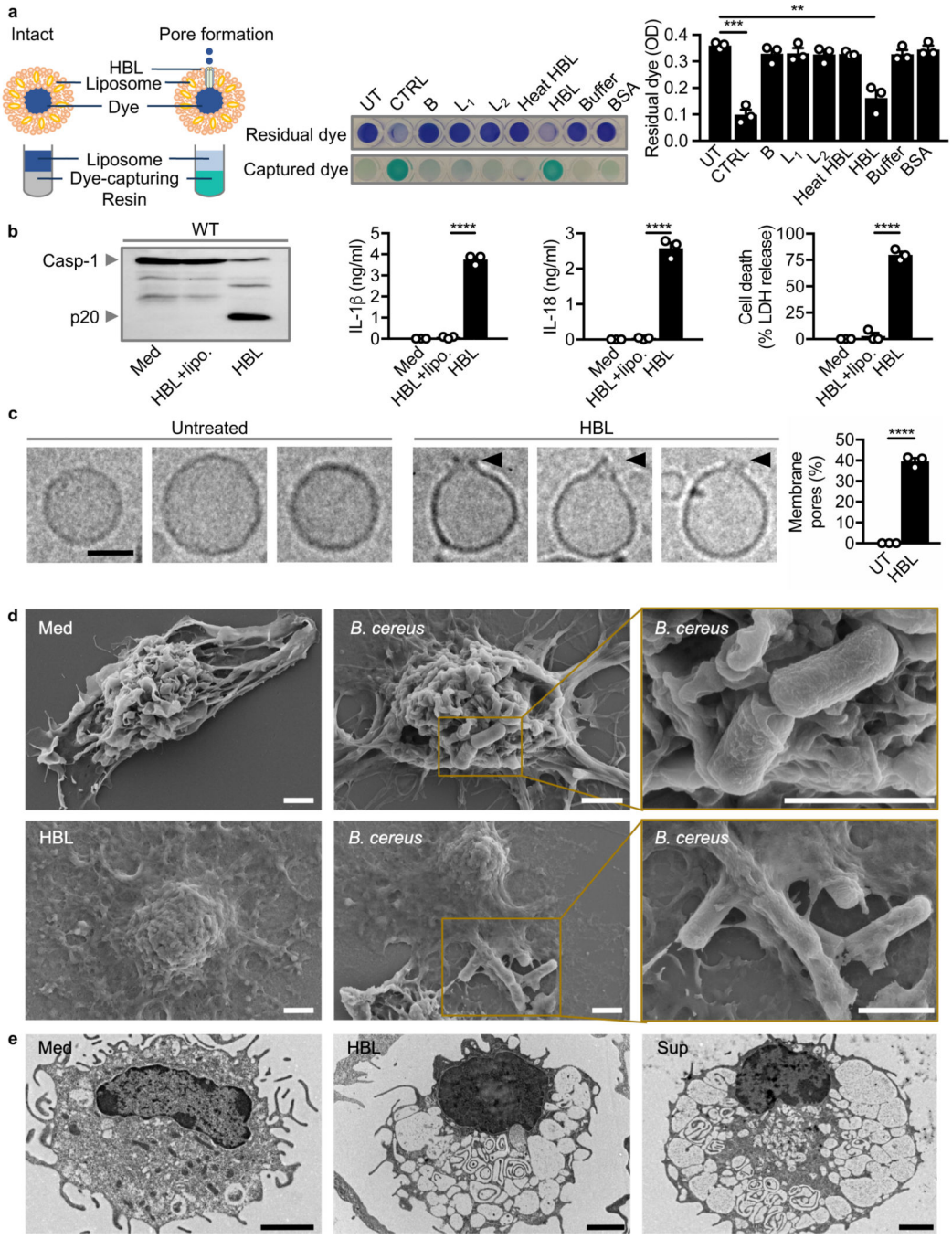


**Fig. 5 |. HBL induces pores on the host cell membrane.**

(**a**) Colorimetric analysis of liposomes left untreated (UT), sonicated for 5 min at 100 amplitude (CTRL), or assessed 30 min after stimulation with individual HBL components, heat-inactivated HBL, HBL, buffer, or BSA. The absorbance (OD) of residual dye was measured at 595 nm. (**b**) Immunoblot analysis of caspase-1 (left), the release of IL-1β (middle-left) and IL-18 (middle-right), and death (right) of WT BMDMs left untreated or assessed 3 hr after stimulation with recombinant HBL in presence or absence of liposomes (lipo.). (**c**) Cryo-EM analysis of liposomes left untreated or assessed 1 hr after stimulation

with recombinant HBL. Images (left) and quantification of percentages of liposomes (right) exhibiting membrane pores in untreated liposomes (n= 469) and HBL-treated liposomes (n= 814). (**d**) Scanning electron microscopy analysis of WT BMDMs left untreated or assessed 3 hr after infection with *B. cereus* (MOI, 5), showing attachment of *B. cereus* to BMDMs or dead BMDMs. Scanning electron microscopy analysis of LPS-primed WT BMDMs assessed 3 hr after stimulation with HBL. (**e**) Transmission electron microscopy analysis of WT BMDMs left untreated or assessed 3 hr after stimulation with HBL or 2 hr after stimulation with the supernatant of *B. cereus* (Sup). Scale bar, 50 nm (c), 2 μm (d and e). Each symbol represents an independent experiment (a-c). $^{**}P < 0.01$, $^{***}P < 0.001$ and $^{****}P < 0.0001$ (one-way analysis of variance [ANOVA] with Dunnett's multiple-comparisons test [a] or two-tailed *t*-test [b and c]). Data are representative of one (d and e) or three independent experiments (n=3 in a-c; mean and s.e.m. in a-c).

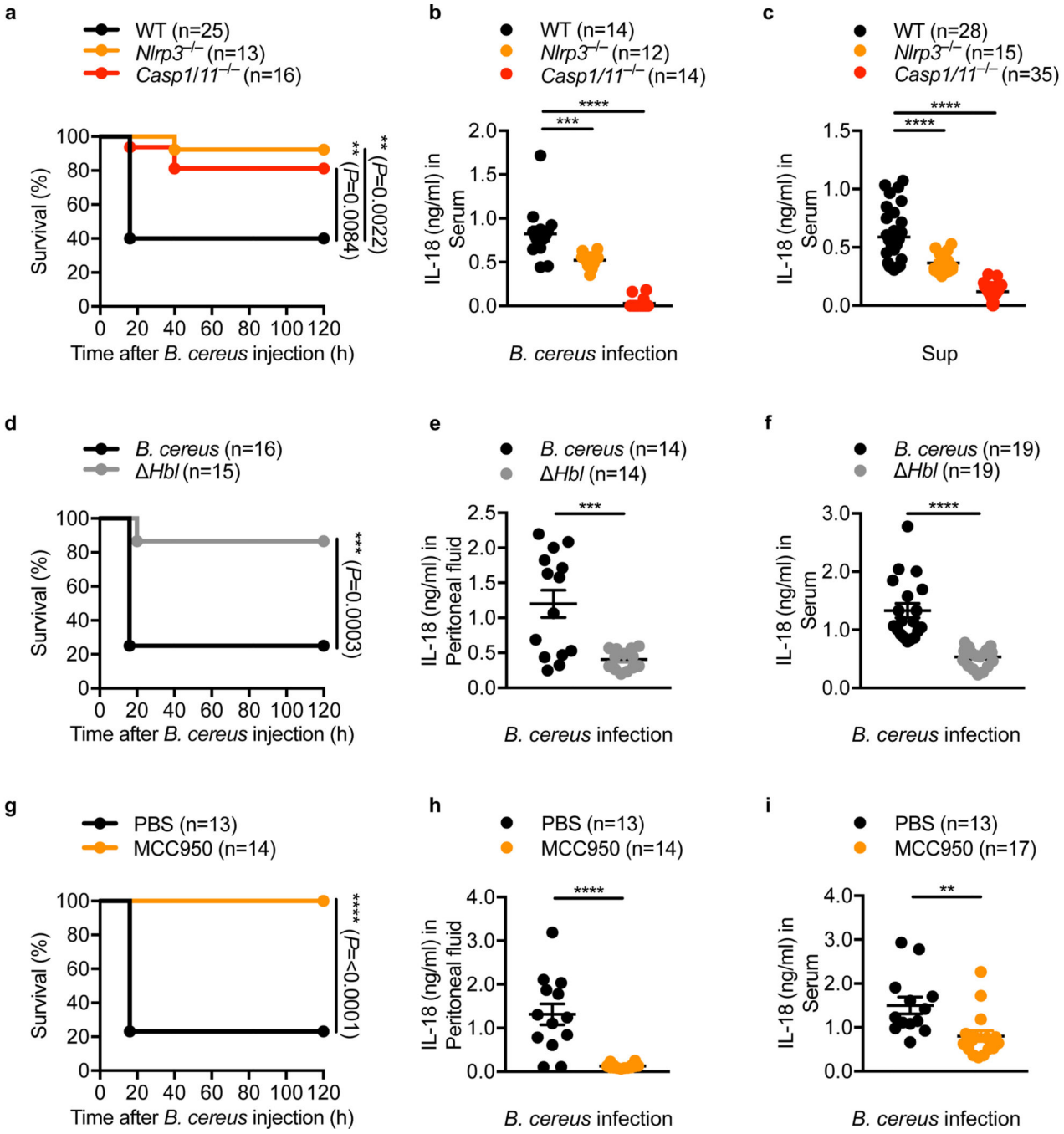


**Fig. 6 |. The NLRP3 inflammasome mediates lethality induced by *B. cereus* infection in vivo.**

(**a**) Survival of WT, *Nlrp3*$^{-/-}$ and *Casp1/11*$^{-/-}$ mice, after intraperitoneal infection with 5 × $10^6$ colony-forming units (CFUs) of *B. cereus*. (**b**) Concentration of IL-18 in the serum of WT, *Nlrp3*$^{-/-}$ and *Casp1/11*$^{-/-}$ mice, 16 hr after intraperitoneal infection with 7.5 × $10^6$ CFUs of *B. cereus*. (**c**) Concentration of IL-18 in the serum of WT, *Nlrp3*$^{-/-}$ and *Casp1/11*$^{-/-}$ mice, 16 hr after intraperitoneal injection with 200 μl of the supernatant of *B. cereus* (Sup). (**d**) Survival of WT mice after intraperitoneal injection with 5 × $10^6$ CFUs either of *B. cereus* ATCC 10876 or of Δ*Hbl B. cereus* (Δ*Hbl*). (**e**) Concentration of IL-18 in the

peritoneal fluid of WT mice, 3 hr after intraperitoneal infection with $7.5 \times 10^6$ CFUs either of *B. cereus* or of Δ*Hbl B. cereus*. (**f**) Concentration of IL-18 in the serum of WT mice, 4 hr after intraperitoneal infection with $7.5 \times 10^6$ CFUs either of *B. cereus* or of Δ*Hbl B. cereus.* (**g**) Survival of WT mice administered either with PBS or with MCC950, both via an intraperitoneal route, followed by intraperitoneal infection with $5 \times 10^6$ CFUs of *B. cereus* with a corresponding second dose of PBS or MCC950. (**h**) Concentration of IL-18 in the peritoneal fluid of WT mice administered with PBS or WT mice administered with MCC950 as in (g), 3 hr after infection with $7.5 \times 10^6$ CFUs of *B. cereus*. (**i**) Concentration of IL-18 in the serum of WT mice administered either with PBS or with MCC950 as in (g), 6 hr after infection with $7.5 \times 10^6$ CFUs of *B. cereus*. Each symbol represents an individual mouse (b, c, e, f, h, i). $^{**}P < 0.01$, $^{***}P < 0.001$ and $^{****}P < 0.0001$ (two-sided log-rank test [a, d and g] or one-way ANOVA with Dunnett's multiple-comparisons test [b and c] or two-tailed *t*-test [e, f, h and i]). Data are pooled from two independent experiments (a, b, and d-i) or from three independent experiments (c, mean and s.e.m. in b, c, e, f, h and i).